Astronomy & Astrophysics manuscript no. cold_disc
March 14, 2017
©ESO 2017

arXiv:1703.04528v1 [astro-ph.HE] 13 Mar 2017

Stable accretion from a cold disc in highly magnetized neutron stars

S. S. Tsygankov[1,2], A. A. Mushtukov[3,2], V. F. Suleimanov[4], V. Doroshenko[4], A. A. Lutovinov[2,5], and J. Poutanen[1,6,7]

[1] Tuorla Observatory, Department of Physics and Astronomy, University of Turku, Väisäläntie 20, FI-21500, Piikkiö, Finland
e-mail: sergey.tsygankov@utu.fi
[2] Space Research Institute of the Russian Academy of Sciences, Profsoyuznaya Str. 84/32, Moscow 117997, Russia
[3] Anton Pannekoek Institute, University of Amsterdam, Science Park 904, 1098 XH Amsterdam, The Netherlands
[4] Institut für Astronomie und Astrophysik, Universität Tübingen, Sand 1, D-72076 Tübingen, Germany
[5] Moscow Institute of Physics and Technology, Moscow region, Dolgoprudnyi, Russia
[6] Nordita, KTH Royal Institute of Technology and Stockholm University, Roslagstullsbacken 23, SE-10691 Stockholm, Sweden
[7] Kavli Institute for Theoretical Physics, University of California, Santa Barbara, CA 93106, USA

Received; accepted

ABSTRACT

Aims. The aim of this paper is to investigate the transition of a strongly magnetized neutron star into the accretion regime with very low accretion rate.
Methods. For this purpose we monitored the Be-transient X-ray pulsar GRO J1008−57 throughout a full orbital cycle. The current observational campaign was performed with the *Swift*/XRT telescope in the soft X-ray band (0.5–10 keV) between two subsequent Type I outbursts in January and September 2016.
Results. The expected transition to the propeller regime was not observed. However, the transitions between different regimes of accretion were detected. In particular, after an outburst the source entered a stable accretion state characterised by the accretion rate of $\sim 10^{14} - 10^{15}$ g s^{-1}. We associate this state with accretion from a cold (non-ionised) disc of temperature below ~ 6500 K. We argue that a transition to such accretion regime should be observed in all X-ray pulsars with certain combination of the rotation frequency and magnetic field strength. Moreover, the propeller effect should never be observed in such sources even for very low mass accretion rates. The proposed model of accretion from a cold disc is able to explain several puzzling observational properties of X-ray pulsars.

Key words. accretion, accretion discs – magnetic fields – stars: individual: GRO J1008−57 – X-rays: binaries

1. Introduction

Properties of the accretion disc strongly depend on parameters of the compact object and binary system as a whole. At the same time, they also determine the observational appearance of an accreting object. As a consequence, some of the physical phenomena typical for one class of objects can be unobservable in another. For instance, transitions between different ionisation states of the accretion disc are commonly considered to be responsible for bright outbursts in dwarf novae and soft X-ray transients (see, e.g., reviews by Cherepashchuk 2000; Lasota 2001; Warner 2003), but previously were not considered for X-ray pulsars (XRPs). The transition is associated with the so called thermal-viscous instability arising due to partial ionisation of hydrogen in the accretion disc (Meyer & Meyer-Hofmeister 1984; Smak 1984; Mineshige et al. 1993; Cheng et al. 1992; Chen et al. 1997).

Ionisation state of plasma in the disc determines its opacity and the equation of state, and, therefore, the viscosity (see e.g. the review by Lasota 2001). In cold disc consisting mainly of atomic hydrogen, the viscosity and thus the accretion rate are low, so the accreted matter accumulates in the disc. In the hot state, the hydrogen is mainly ionised and the disc viscosity dramatically increases, which allows most of the accumulated matter to be rapidly accreted onto a compact object. The critical effective temperature defining the two states is hydrogen ionisation temperature ~ 6500 K (see Sec. 3.5 in Warner 2003). Transition between the two states is accompanied by a heating wave originating either from its inner or outer part of the accretion disc (Smak 1984). The accretion process becomes stable again when the temperature falls for some reason below the critical value over the entire disc, i.e. in the case of the low mass accretion rate (Lasota 1997),

$$\dot{M} < \dot{M}_{\rm cold} \simeq 3.5 \times 10^{15}\, r_{10}^{2.65}\, M_{1.4}^{-0.88} \quad {\rm g\,s^{-1}}, \tag{1}$$

where r_{10} is the inner disc radius[1] and $M_{1.4}$ is the neutron star mass in units of $1.4 M_\odot$.

In the case of rapidly rotating accreting XRPs (using 4U 0115+63 and V 0332+53 as case studies), Tsygankov et al. (2016a) showed that observation of transition of the accretion disc to the cold state is impossible because of the onset of the propeller regime at much higher mass accretion rates compared to that required for the accretion disc to have temperature below 6500 K at the inner radius. At the same time the overall shape and energetics of the outburst were shown to correspond to expectations from the disc instability model.

XRPs with spin periods sufficiently long to reduce the centrifugal barrier are required to reach the sufficiently low mass accretion rate to switch the accretion disc to the cold state before the transition to the propeller regime. A few XRPs with long spin

[1] We define $Q_x = Q/10^x$ in cgs units if not mentioned otherwise.

periods exist with one of them, GRO J1008−57, showing very predictable Type I outbursts every periastron passage with long quiescence periods between the outbursts (Kühnel et al. 2013). This source was selected for the monitoring campaign covering a full orbital cycle and aimed to study the source properties at a very low mass accretion rate.

GRO J1008−57 was discovered as an XRP with a period of 93.587 ± 0.005 s by BATSE instrument onboard the *Compton Gamma-Ray Observatory* (*CGRO*) during the bright outburst in 1993 (Stollberg et al. 1993). Its transient nature was associated with the Be type of the optical companion (B1-B2 Ve star; Coe et al. 2007). GRO J1008−57 demonstrates both giant, Type II, and Type I (associated with the periastron passage) outbursts. Distance to the source was estimated to be 5.8 kpc (Riquelme et al. 2012). The orbital parameters of the binary system were determined using the data from several observatories: orbital period $P_{\rm orb}$ = 249.46 ± 0.10 d, projected semi-major axis $a_{\rm x}$ sin i = 530 ± 60 lt-s, longitude of periastron ω = −26 ± 8 deg, and the eccentricity e = 0.68 ± 0.02 (Levine & Corbet 2006; Coe et al. 2007; Kuehnel et al. 2012). The presence of a cyclotron line at ∼ 88 keV in spectrum of the source was first suggested based on the *CGRO*/OSSE data (Shrader et al. 1999) and later confirmed with *Suzaku* at $E_{\rm cyc}$ = 75.5 keV (Yamamoto et al. 2013). This allows us to estimate the magnetic field of the neutron star of $\sim 8 \times 10^{12}$ G.

In this work we analyse the data obtained with the *Swift*/XRT telescope during one full orbital cycle of Be/XRP GRO J1008−57 between the two consequent Type I outbursts in January and September 2016. Unique combination of high sensitivity and flexibility of scheduling for the *Swift* observatory allowed us to perform detailed long-term observational campaign aimed on reaching accretion regimes never investigated before. Knowledge of the magnetic field strength of the neutron star as well as of other parameters of the system allowed us to interpret the observed temporal behaviour in terms of the accretion disc instability and to construct the model of accretion from a cold disc in highly magnetized neutron stars.

2. Data analysis and results

2.1. Swift/XRT observations

Swift observatory (Gehrels et al. 2004) gives a possibility to perform long-term campaigns of observations of faint X-ray sources using the focusing XRT telescope (Burrows et al. 2005) onboard. This work is based on the XRT data collected between two consequent Type I outbursts in January and September 2016 (Kretschmar et al. 2016; Nakajima et al. 2016). Observations were performed every 3–4 days in Photon Counting (PC) mode. The spectrum in each observation was extracted using the online tools[2] provided by the UK Swift Science Data Centre (Evans et al. 2009).

Spectra were fitted in XSPEC package using the Cash statistic (Cash 1979) after they were grouped to have at least 1 count per bin. To avoid any problems caused by the calibration uncertainties at low energies,[3] we restricted our spectral analysis to the 0.7–10 keV band.

To estimate the bolometric correction factor we used the results obtained by Kühnel et al. (2013) who demonstrated the dependence of the source spectrum on its luminosity. Using the spectral parameters in the faint state of GRO J1008−57 we obtained an estimate for the bolometric correction factor $K_{\rm bol}$ ∼ 1.6. We note that remaining uncertainty in the correction factor does not influence any of the conclusions. In the following analysis we apply this correction to the *Swift*/XRT data and refer to the bolometric fluxes and luminosities, unless stated otherwise.

[2] http://www.swift.ac.uk/user_objects/

[3] http://www.swift.ac.uk/analysis/xrt/digest_cal.php

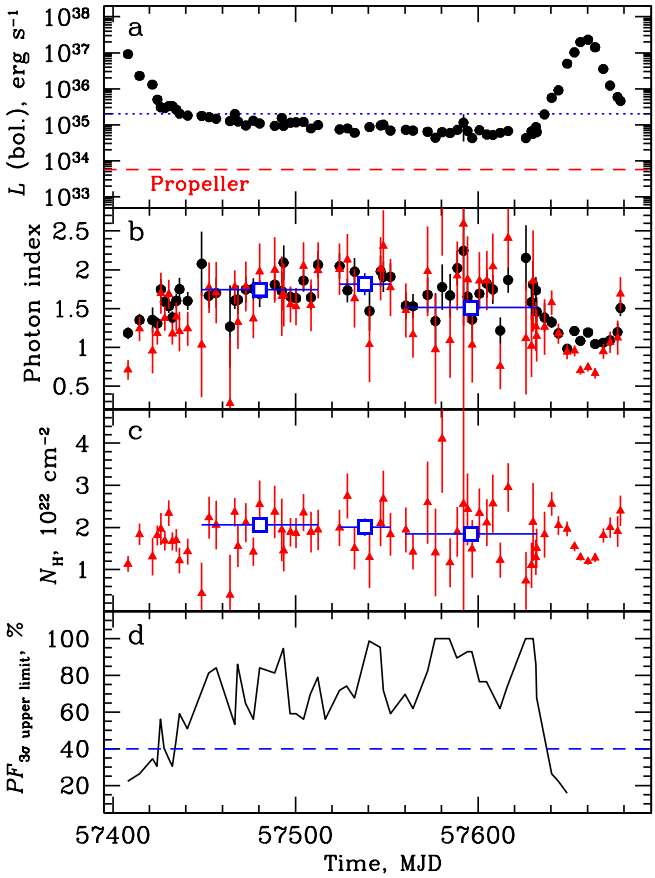

Fig. 1. (a) The bolometric luminosity of GRO J1008−57 obtained by the *Swift*/XRT telescope. Luminosity is calculated from the unabsorbed flux under assumption of the distance d = 5.8 kpc and fixed $N_{\rm H} = 2.0 \times 10^{22}$ cm^{-2}. The dashed red and dotted blue lines show the predicted luminosity $L_{\rm prop}$ for the transition to the propeller regime and observed transition to the low-level stable accretion regime, respectively. Panels (b) and (c) represent variations of the photon index and absorption value with time, respectively. Black symbols correspond to the fixed $N_{\rm H}$, red triangles and blue open squares – to the absorption as a free parameter. In panel (d) the estimated 3σ upper limits for the pulsed fraction as function of time are shown for the *Swift*/XRT data with the horizontal dashed line showing the typical pulsed fraction measured during the bright state. The pulsations are clearly detected in all observations which are expected to be sufficiently sensitive (i.e. below this line), but not elsewhere.

2.2. Timing analysis

The light curve of GRO J1008−57 obtained from the *Swift*/XRT data is shown in Fig. 1. Originally the observations were requested in order to detect the transition of GRO J1008−57 to the propeller regime (see Section 3) at the limiting luminosity of $L_{\rm prop} = 5.6 \times 10^{33}$ erg s^{-1} (shown in the upper panel of Fig. 1 with the horizontal dashed line). However, at some point in the declining phase of the outburst the source surprisingly stopped fading around MJD 57440 at the luminosity around 10^{35} erg s^{-1} (shown in the same figure with dotted line), which is one and a half orders of magnitude higher than $L_{\rm prop}$. During the next

seven months the source continued to fade but with much lower rate characterised by e-folding time of $\tau \sim 145$ days in contrast to $\tau \sim 5.5$ days before the transition. Strictly speaking, the flux decline during the low-level state is better fitted with the power-law of index ~ -0.7.

Eventually the monitoring covered the whole orbital cycle with the sharp brightening of the source on MJD 57648 signifying the next Type I outburst during the subsequent periastron passage (Nakajima et al. 2016). The transition of the source to the propeller state thus has not been observed.

2.2.1. Pulsations

Despite short duration of individual *Swift* observations and long spin period of the source, the pulsations are easily detectable during the outburst. Similarly to earlier reports (Kühnel et al. 2013; Bellm et al. 2014) the pulse profile exhibits two peaks with relatively high pulsed fraction of 40−50%, that is typical for most of XRPs (Lutovinov & Tsygankov 2009). However, no pulsation were detected after the observation 00031030034 (MJD 57430.51), when source entered low-level stable accretion state. On the other hand, number of photons per observation becomes too low at this stage (few tens to few hundreds), so non-detection of the pulsations might be simply due to the insufficient counting statistics. Indeed, for all low-level observations the 3σ upper limits for amplitude of the pulsations calculated based on the H-test (de Jager et al. 1989) and following the approach described in Brazier (1994) lie in range 40−95%, as illustrated in Fig. 1d. The non-detection of the pulsations in individual *Swift* observations at low fluxes is, therefore, expected taking into the account their sensitivity to pulsed flux.

On the other hand, search for the pulsations in the combined light-curve is complicated by the sparse sampling of the light curve and uncertainty in orbital parameters of the system. We conclude, therefore, that non-detection of the pulsations by *Swift* does not contradict presence of pulsations given the available counting statistics and light curve sampling.

Somewhat stronger limits on the amplitude of the pulsations in the quiescence can be obtained from 5 ks long *Chandra* observation 14639 of the source carried out in May 2013 (MJD 56440.72) between the Type I outbursts. The bolometric luminosity calculated in the same way as for *Swift* data is $\sim 10^{35}$ erg s^{-1}, i.e. comparable with the values measured by *Swift* during our observations in the low-level stable state. To search for the pulsations we first extracted photons from a circle with radius 7.4″ centered on the source position after applying the standard screening criteria described in instruments documentation. This yields 3215 source photons, which is actually comparable to that for individual *Swift*/XRT observations during the outburst and only factor of two less than total number of photons detected by *Swift* in the low-level state. On the other hand *Chandra* observation is not affected by the uncertainty in orbital parameters. To search for the pulsations we first correct photon arrival times for the effects of orbital motion in solar and binary systems using ephemeris reported by Kühnel et al. (2013) and then use the same approach as for *Swift* data. No significant pulsations around the source pulse frequency could be detected with the 3σ upper limit of $\sim$ 20% for periods in range 80−100 s. Note, however, that *Chandra* data is susceptible to pile-up which potentially reduces sensitivity to pulsed flux. The pile-up fraction is lower for pixels in the wings of the point-spread function and higher in its core, i.e. depends on count-rate in a given pixel. Therefore, we repeated the simulation above for each pixel within circle with radius of 10 pixels centered on the source. All events detected within a single frame (3.2 s) were considered as one event and noted to estimate total pile-up fraction, which turned out to be around $\sim$ 15%. The upper limit on pulsed fraction was then estimated using concatenated event list from all pixels as described above, and indeed turned out to be significantly higher at $\sim$ 35%. While slightly lower than typical pulsed fraction observed during the outburst, this by no means excludes pulsations at low fluxes, especially considering the fact that the pulsed fraction is known to be variable and that we ignored background for this estimate. We conclude, therefore, that additional observations, preferably with *XMM-Newton*, are required in order to study the pulsations in low-level stable accretion regime.

2.3. Spectral variability

All spectra from individual observations can be fitted with the simple absorbed power-law model. To illustrate the stability of the spectral shape over the luminosity and time, in Fig. 2 we present three spectra of GRO J1008−57 obtained in the brightest state of the January 2016 outburst (ObsId 00031030028; red circles), around the transition luminosity (ObsId 00031030035; blue squares), and deep inside the stable low-level state (ObsIds 00031030066-85; magenta crosses) with luminosities 6.9×10^{36}, 3.1×10^{35} and 5.7×10^{34} erg s^{-1}, respectively. No significant differences are immediately suggested by the data.

More detailed analysis, however, reveals a minor change in the absorption and photon index values in the data collected in the bright (outburst) and low-level states. To get sufficient count statistics in the low-level state (between MJD 57440 and 57630) we binned the available data into three wide bins (see Fig. 1 and Table 1).

As a result we found that during the outburst (before MJD 57440 and after MJD 57648) the mean value of $N_{\rm H}$ is less than $\sim 1.8 \times 10^{22}$ cm^{-2} which is just slightly higher than the Galactic value in this direction ($N_{\rm H} = 1.4 \times 10^{22}$ cm^{-2}; Kalberla et al. 2005). On the other hand, after the transition its value increases up to $N_{\rm H} = (2.0 \pm 0.1) \times 10^{22}$ cm^{-2}. The difference is most prominent in the parameters of averaged spectra. Variability of the spectral parameters during the whole orbital cycle of GRO J1008−57 is shown in Fig. 1 for single and averaged observations. Middle and bottom panels illustrate variations of the photon index and absorption column with time, respectively. Black symbols correspond to the absorption column fixed at $N_{\rm H} = 2.0 \times 10^{22}$ cm^{-2}, while red triangles and blue open squares to the fits with free absorption.

The observational log as well as the best-fit spectral parameters for single and averaged observations are presented in Table 1 for both free and fixed absorption values.

3. Discussion

Accreting magnetized neutron stars (XRPs, accreting millisecond pulsars, accreting magnetars) exhibit complex behaviour determined by interaction of their magnetospheres with the accreting matter. Particularly, at very low mass accretion rates the so-called "propeller effect" may occur as abrupt luminosity drop below some critical value (Illarionov & Sunyaev 1975). This rapid cease of accretion is caused by a centrifugal barrier produced by the rotating magnetosphere if it moves faster than the local Keplerian velocity (in another words if magnetospheric radius $R_{\rm m}$ is larger than the corotation radius $R_{\rm c}$).

The limiting luminosity for the onset of the propeller can be estimated by equating the corotation and magnetospheric radii

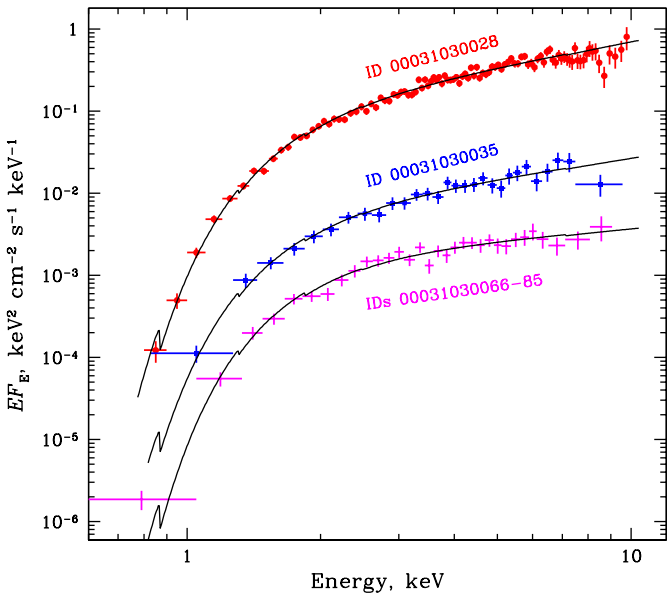

Fig. 2. The spectra of GRO J1008−57 obtained by *Swift*/XRT in different luminosity states: the brightest state of the January 2016 outburst (ObsId 00031030028; red circles), transiting luminosity (ObsId 00031030035; blue squares), deep inside the stable low-level state (ObsIds 00031030066-85; magenta crosses).

(see, e.g., Tsygankov et al. 2016a):

$$L_{\rm prop} \simeq \frac{GM\dot{M}_{\rm prop}}{R} \simeq 4\times10^{37} k^{7/2} B_{12}^2 P^{-7/3} M_{1.4}^{-2/3} R_6^5 \,{\rm erg\ s^{-1}}, \quad (2)$$

where P is the neutron star rotational period in seconds and $\dot{M}$ is the mass accretion rate. Factor k accounts for the details of interaction of the accretion flow with magnetosphere relating its size to the Alfvén radius, i.e. $k = R_{\rm m}/R_{\rm A}$. In the case of disc accretion it is usually assumed to be $k = 0.5$ (Ghosh & Lamb 1978).

Observational evidence for the propeller effect were found in a number of sources with magnetic fields from $\sim 10^8$ G (for the accreting millisecond pulsar SAX J1808.4–3658; Campana et al. 2008) to $\sim 10^{14}$ G (for the first pulsating ULX M82 X-2; Tsygankov et al. 2016b). The XRPs typically have magnetic fields somewhere in between these values, and some of them also exhibit transition to the propeller regime (Stella et al. 1986; Cui 1997; Campana et al. 2001; Tsygankov et al. 2016a; Lutovinov et al. 2017).

Our observational campaign was originally aimed at the detection of the transition of GRO J1008−57 to the propeller regime. In the case of GRO J1008−57 equation (2) gives $L_{\rm prop} = 5.6\times10^{33}$ erg s^{-1}. However, instead of sharp drop of the flux GRO J1008−57 entered a stable accretion regime at the luminosity around 10^{35} erg s^{-1} (see Fig. 1), about one and a half orders of magnitude higher than $L_{\rm prop}$.

Note that unlike V 0332+53 and 4U 0115+63 where an obvious spectral softening was observed after the transition to the propeller regime (Tsygankov et al. 2016a), no such changes have been observed in GRO J1008−57 after the transition to the stable accretion state. This strongly suggests that the emission mechanism remains the same, i.e. the source continues to accrete. Another argument to support this conclusion is associated with the observed spin evolution of the source between the outbursts, i.e. the spin-up at average rate of $\dot{P} = -2.4(5)\times10^{-9}$ s s^{-1} observed between the outbursts (see Sec. 3.4.1 for the details). The observed spin-up of the neutron star can only be explained by continuing accretion, i.e. the source does accrete also during in quiescence. Below we discuss this behaviour in terms of the accretion disc transition to the cold (neutral) state allowing stable accretion at very low rates.

3.1. Accretion disc instability

As was shown by Lasota (1997) stable accretion to the compact object is possible if the mass accretion rate is high enough to keep the entire accretion disc hot and fully ionised (temperature > 6500 K) or if the mass accretion rate is so low, that the temperature is below the critical value even at the inner radius. At intermediate levels of the mass accretion rate the appearance of the region with temperature of 6500 K will cause a rapidly propagating heating or cooling front through the disc leading to the fast variability of the source flux. In this Section we will put the XRPs into the context of the disc instability model and make predictions for the pulsars with different properties (see also discussion in Tsygankov et al. 2016a).

Let us consider conditions under which an XRP may accrete matter from the recombined (cold) disc. Particularly, two criteria have to be fulfilled: (1) the mass accretion rate has to be high enough to allow the matter to penetrate through the centrifugal barrier, and at the same time (2) the mass accretion rate has to sufficiently low to allow the disc to remain sufficiently cold ($<$ 6500 K) at every radius.

The first criterion was already discussed above and is realized if the magnetospheric radius $R_{\rm m}$ is smaller than the corotation radius $R_{\rm c}$:

$$R_{\rm m} \le R_{\rm c}. \quad (3)$$

The magnetospheric radius is

$$R_{\rm m} \simeq 2.5\times10^8\, k\, M_{1.4}^{1/7} R_6^{10/7} B_{12}^{4/7} L_{37}^{-2/7} \quad {\rm cm}. \quad (4)$$

The neutron star magnetic momentum is taken to be $\mu = BR^3/2$. The corotation radius is:

$$R_{\rm c} = \left(\frac{GMP^2}{4\pi^2}\right)^{1/3} \simeq 1.68\times10^8\, M_{1.4}^{1/3} P^{2/3} \quad {\rm cm}. \quad (5)$$

The condition (3) is fulfilled when the accretion luminosity is higher than the threshold luminosity presented above (see Eq. 2): $L \ge L_{\rm prop}$.

The second criterion is satisfied if the mass accretion rate is below the value given by Eq. (1) ($\dot{M} < \dot{M}_{\rm cold}$; Lasota 1997). Substituting the magnetospheric radius instead of r into Eq. (1) we obtain another condition for the stable accretion from a cold disc:

$$L < L_{\rm cold} = 9\times10^{33}\, k^{1.5} M_{1.4}^{0.28} R_6^{1.57} B_{12}^{0.86} \quad {\rm erg\,s^{-1}}. \quad (6)$$

Below this level the temperature in the accretion disc is lower that 6500 K at $R > R_{\rm m}$.

If the threshold luminosity for the propeller regime is higher than the luminosity corresponding to transition to the cold disc ($L_{\rm prop} > L_{\rm cold}$) then the decrease of the mass accretion rate during the outburst decay will trigger the transition to propeller. In the opposite case ($L_{\rm prop} < L_{\rm cold}$) the accretion disc will switch to the cold state with low viscosity, allowing stable accretion even at very low rate.

Interestingly, the final state of the source after an outburst is determined by two fundamental parameters of the neutron star:

magnetic field and spin period. Equating the expressions for luminosities $L_{\rm cold}$ and $L_{\rm prop}$ one can derive the critical value of the spin period as a function of the neutron star magnetic field:

$$P^* = 36.6\, k^{6/7}\, B_{12}^{0.49}\, M_{1.4}^{-0.17}\, R_6^{1.22} \quad \text{s}. \tag{7}$$

If the spin period $P < P^*$, a pulsar will end up in the propeller regime. Otherwise, the source will start to accrete stably from the cold disc.

3.2. More accurate condition for the accretion from a cold disc

The condition given by Eq. (6) is based on the assumption that disc temperature is highest at the inner radius given by $R_{\rm m}$. However, effective temperature distribution over the radial coordinate depends on the exact boundary condition and viscous stress at the magnetospheric radius. The condition (6) can be derived more accurately. There is an uncertainty in the location, where the stress disappears. This uncertainty is described by parameter β: $\beta = 1$ corresponds to a disappearance of the stress at the magnetospheric radius $R_{\rm m}$, while $\beta = 0$ corresponds to the case when the stress disappears at $r \ll R_{\rm m}$. Then the distribution of effective temperature $T_{\rm eff}$ over the radial coordinate is given by (Frank et al. 2002):

$$\sigma_{\rm SB} T_{\rm eff}^4 = \frac{3}{8\pi}\frac{L}{r^3} R \left[1 - \beta\left(\frac{R_{\rm m}}{r}\right)^{1/2}\right], \tag{8}$$

where $\sigma_{\rm SB}$ is the Stefan-Boltzmann constant. The maximum effective temperature,

$$\sigma_{\rm SB} T_{\rm eff,max}^4 = A\,\frac{3}{8\pi}\frac{L}{R_{\rm m}^3} R, \tag{9}$$

is achieved at the radius

$$r_{\rm max} = \begin{cases} \dfrac{49}{36}\beta^2 R_{\rm m}, & \text{if} \quad \beta \geq \dfrac{\sqrt{3}}{2}, \\ R_{\rm m}, & \text{if} \quad \beta < \dfrac{\sqrt{3}}{2}, \end{cases} \tag{10}$$

where

$$A = \begin{cases} 0.057\,\beta^{-6}, & \text{if} \quad \beta \geq \dfrac{\sqrt{3}}{2}, \\ 1 - \beta, & \text{if} \quad \beta < \dfrac{\sqrt{3}}{2}. \end{cases} \tag{11}$$

As a result, condition (6) can be rewritten in more accurate way. In this approach the maximum effective temperature in the disc is less than 6500 K all over the disc if the accretion luminosity is

$$L \leq L_{\rm cold}^{(2)} \simeq 7\times10^{33} A^{-7/13}\, k^{21/13}\, M_{1.4}^{3/13}\, R_6^{23/13}\, B_{12}^{12/13}\, T_{6500}^{28/13} \ \text{erg s}^{-1}, \tag{12}$$

where $T_{6500} = T_{\rm eff}/6500$ K. This estimate is more accurate than Eq. (6) as it accounts for interaction of disc with the magnetosphere. In the case when the stress disappears at $R_{\rm m}$ the condition (12) gives $L_{\rm cold}$ higher by a factor of few than Eq. (6).

Using the updated Eq. (12) for critical accretion luminosity $L_{\rm cold}^{(2)}$ we can derive an updated equation for the critical value of spin period P^* which, as was mentioned above, determines the pulsar behaviour at very low mass accretion rate. Now instead of Eq. (7) we have:

$$P^* = 40.7\, k^{21/23}\, B_{12}^{6/13}\, M_{1.4}^{-5/13}\, R_6^{18/13}\, A^{3/13}\, T_{6500}^{-12/13} \quad \text{s}. \tag{13}$$

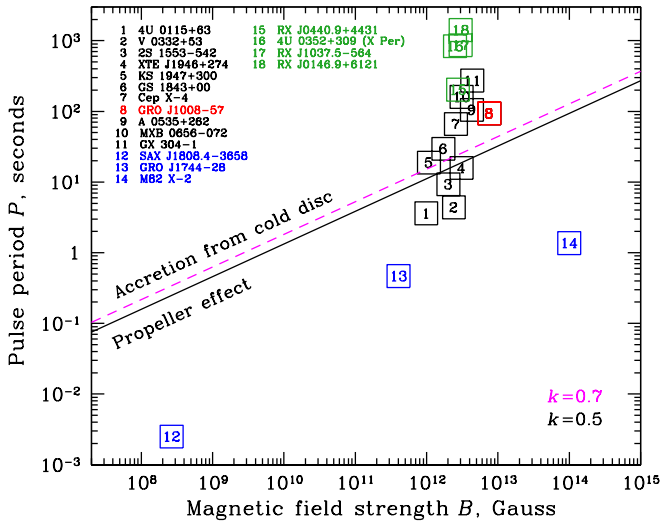

Fig. 3. Collection of some known BeXRPs (shown with the black colour), as well as the accreting millisecond pulsar SAX J1808.4−3658, the intermediate pulsar GRO J1744−28 and the accreting magnetar M82 X-2 (all three shown with the blue colour) on the $B-P$ plane. The solid and dashed lines correspond to the prediction of $P^*(B)$ from Eq. (13) for $\beta = 1$ and two different values of parameter k: 0.5 and 0.7, respectively. This line separates sources where propeller regime is possible from ones with stable accretion from the cold disc. Persistent low-luminous BeXRPs are shown with green colour. GRO J1008−57 is coloured in red and resides in the area corresponding to the sources with accretion from the cold disc.

This equation can be used to predict the behaviour of any XRP (with known magnetic field) expected in the case of transient activity. Especially it is important for XRPs in Be binary systems (BeXRPs), known to be transient sources (see, e.g., Reig 2011) with magnetic fields measured from the cyclotron lines in their spectra (Walter et al. 2015). For the illustration we put some known BeXRPs, as well as the accreting millisecond pulsar SAX J1808.4−3658, the intermediate pulsar GRO J1744−28 and the accreting magnetar M82 X-2 on the $B-P$ plane in Fig. 3. All sources in this plane are divided with the prediction from Eq. (13) into two groups: (i) ones entering the propeller regime at low mass accretion rate (below the line), and (ii) sources where stable accretion from the cold disc shall continue at any accretion rate (above the line). Persistent low-luminous BeXRPs (Reig & Roche 1999) are shown with the green colour. Clearly GRO J1008−57 resides in the area corresponding to the sources with accretion from the cold disc. The majority of sources residing below the $P^*(B)$ line were already shown to exhibit the transitions to the propeller regime (for a review see Tsygankov et al. 2016a).

It is worth mentioning that sources above the line, i.e. sources switching to the accretion from the cold disc, will never transit to the propeller regime due to very specific dependence of the inner radius of the disc on the decreasing mass accretion rate (see below).

3.3. Interaction of a cold disc with magnetosphere

The inner radius of the accretion disc is conventionally defined by its interaction with magnetosphere and, to a first approximation, can be estimated from equality of the magnetic pressure and the ram pressure of the matter in the azimuthal direction (for more details see, e.g., D'Angelo & Spruit 2010). As a result, the

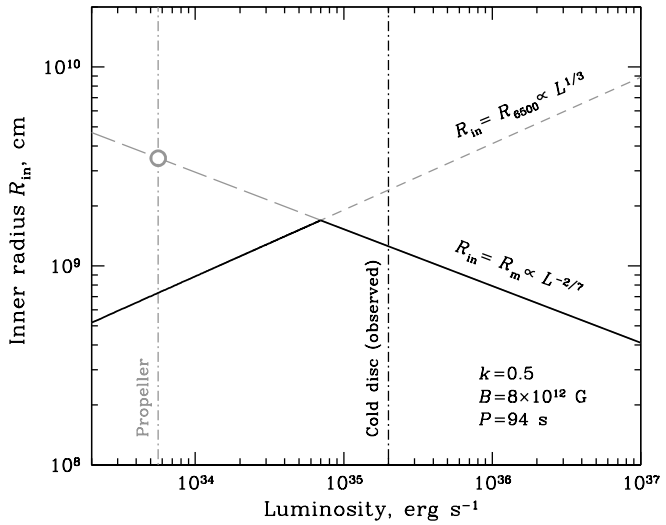

Fig. 4. The inner disc radius as a function of luminosity (black solid line). At high mass accretion rate the inner disc radius coincides with the magnetospheric radius (Eq. 4; shown with long-dashed line). At low mass accretion rate the disc is cold and can penetrate deeper into the neutron star magnetosphere until its temperature reaches 6500 K (Eq. 14; shown with short-dashed line). Observed bolometric luminosity of transition to the stable low-level accretion from the cold disc is shown with black dot-dashed line. Grey dot-dashed line demonstrates the prediction for the propeller effect threshold luminosity $L_{\rm prop}$.

inner disc radius is given by Eq. (4). However, this scenario implies that the matter in the accretion disc is highly ionised. Otherwise the interaction with magnetic field is not effective.

If this is the case, the disc can penetrate deeper into the magnetosphere and the magnetospheric radius will be determined by the disc radius, where the effective temperature will reach 6500 K and the disc will transit to a highly ionised state. This radius can be easily found from Eq. (8):

$$R_{6500} \simeq 2.3 \times 10^{10} A^{1/3} L_{37}^{1/3} R_6^{1/3} \quad \text{cm}. \tag{14}$$

At lower radii the disc becomes highly ionised and follows magnetic field lines. In reality the situation can be more complicated because the interaction of the accretion disc and neutron star magnetic field can affect the temperature structure of the accretion disc.

Finally, we come to a very interesting conclusion: at high mass accretion rate the inner disc radius is determined by the equality of the magnetic pressure and the azimuthal ram pressure. This radius increases with the decreasing of the mass accretion rate according to Eq. (4). If the mass accretion rate reaches the critical value given by Eq. (12), i.e. disc switches to the cold state, the inner disc radius is defined by the radius where the temperature reaches 6500 K. It is given by Eq. (14) and decreases with the decrease of the mass accretion rate. In this situation the inner radius will not reach the corotation radius and thus pulsar will never switch to the propeller regime.

This picture is illustrated in Fig. 4 where the inner disc radius as a function of luminosity is presented (solid black line). At high mass accretion rate the inner disc radius coincides with the magnetospheric radius (Eq. (4); shown with long-dashed line). At low mass accretion rate the disc is cold and can penetrate deeper into neutron star magnetosphere. In this case its inner radius is defined by the condition where the disc temperature is 6500 K (Eq. (14); shown with short-dashed line). The observed bolometric luminosity ($\sim 2 \times 10^{35}$ erg s^{-1}) of GRO J1008−57 transition to the stable low-level accretion from the cold disc is shown with black dot-dashed line. Grey dot-dashed line demonstrates the prediction for the propeller effect threshold luminosity $L_{\rm prop}$ under assumption of the inner radius follows Eq. (4) down to such low mass accretion rate.

As can be seen from Fig. 4 our prediction of the transition to the accretion from the cold disc coincides with the observed value within the factor of 2–3. Taking into account existing systematic uncertainties (distance to the system, physics of coupling between the disc and the star, width of the coupling region, uncertainty in the transiting temperature) we consider this match as a support of our physical picture.

Another possible source of uncertainty is irradiation of the accretion disc by the central object. However, we do not expect a strong influence of the neutron star emission. Indeed, according to the existing computations for the cold parts of the discs, their relative thickness h/r is significantly smaller than the corresponding value for the hot parts (see, e.g., Meyer & Meyer-Hofmeister 1982). Moreover, the relative thickness of cold convective disc rapidly decreases with radius. This implies that the outer regions of the cold accretion disc are in the shadow of the inner hot ring and are not affected at all by the hard radiation from the central source. The irradiation can affect, however, the temperature of the inner accretion disc which could lead to slight underestimation of the magnetospheric radius for the cold disc presented above. However, the overall behaviour as a function of the mass accretion rate will be as predicted in our model.

3.4. Observational appearance

3.4.1. Neutron star spin-up / spin-down

Acceleration/deceleration of the neutron star rotation is determined mainly by two parameters: mass accretion rate and the inner radius of the accretion disc where it interacts with the magnetosphere. In our model we show that some pulsars may depart from the classical dependence of the inner radius of the disc given by magnetospheric radius at low mass accretion rates. Moreover, they will not switch to the propeller regime, when neutron star is effectively decelerated. Instead of that cold accretion disc can come close to the neutron star transferring its angular momentum to the central object.

Indeed, the long-term spin history of GRO J1008−57 as observed by *Fermi*/GBM[4] suggests that unlike most of the Be transients, this source does indeed spin-up between the outbursts. The corresponding spin-up rate can be estimated by comparing the last and the first measured spin frequencies of the consequent Type I outbursts corrected for orbital motion using ephemeris reported by Kühnel et al. (2013). We estimate mean spin-up rate at $\dot{P} = -2.4(5) \times 10^{-9}$ s s^{-1} where the uncertainty corresponds to standard deviation of values measured for individual outbursts.Note that not only the observed spin-up rate is rather high, but it is also consistent for all quiescent periods.

This strongly suggests that the accelerating torque is always acting onto the neutron star when it is accreting at low luminosities. The fact that the observed spin-up rate is remarkably stable (as follows from low dispersion of the values observed for individual quiescent periods) implies that the accretion rate was also stable during these periods, which is fully consistent with the cold accretion disc model. We also note that it is clear that the discussed effect can potentially strongly affect the spin evolution

[4] http://gammaray.msfc.nasa.gov/gbm/science/pulsars/lightcurve

of XRPs and has to be taken into account, for example, for the estimates of equilibrium periods.

3.4.2. Power spectrum

Power spectra of XRPs are usually characterized by the power-law shape $P \propto f^{-1...-1.5}$ up to the maximal frequencies generated in the disc. The fluctuations are caused by initial fluctuations arising at different radii due to magnetohydrodynamic turbulence (Balbus & Hawley 1991) and propagating inwards due to viscous diffusion (Lyubarskii 1997). In the case of the cold accretion disc the initial fluctuations are strongly suppressed and the final rms of X-ray flux fluctuations is expected to be very small. The cold disc can produce strong initial fluctuations of the mass accretion rate only at its inner radius, where temperature reaches 6500 K. As a result, the power spectrum density will be described by a constant cutting off at a typical frequency corresponding to the inner disc radius, which is its local Keplerian frequency (Revnivtsev et al. 2009). If the accretion disc is cold and penetrates deep into the magnetosphere the break frequency should be higher than the Keplerian frequency at the magnetospheric radius R_m calculated for a given mass accretion rate using Eq. (4). Unfortumately, low count rate observed from GRO J1008−57 does not permit us to verify this prediction, however, it is in principle verifyable with the additional dedicated observations with *XMM-Newton*.

3.4.3. Unstable accretion

Depending on mass accretion rate in the disc and disc properties, the accretion process from a cold disc can be either stable or unstable. Indeed, if the temperature on the inner edge of the disc is less than ~ 6500 K the matter can be accumulated there until the local temperature reaches this critical value. After that the locally increased viscosity allows the inner region of the disc to accrete sporadically on to the neutron star. A similar mechanism was proposed earlier to explain bright flares in GRO J1744−28, but the local increase of viscosity was associated with transitions of the inner part of the disc to the radiation-pressure dominated regime (Cannizzo 1996).

3.4.4. Luminosity decay in the cold disc state

GRO J1008−57 shows gradual decay of the mass accretion rate in the cold accretion disc state (see upper panel of Fig. 1). The decay is described by the power-law: $L \propto \dot{M} \propto t^{-p}$, where $p \approx 0.7$. The viscous diffusion defining the decay law can be described by Green's functions specified by appropriate conditions in the disc (Lynden-Bell & Pringle 1974; Tanaka 2011; Lipunova 2015). The mass accretion rate evolution at the inner disc radius is determined by initial geometrical size of a disc and its viscosity. The observed decay reflects the evolution of the accretion disc and can be used for diagnostics of the disc in the cold state.

3.4.5. Pulsations and energy spectrum

The decrease of the pulsed fraction observed after the transition to the cold disc state (see Section 2.2.1) can be explained by the increase of the polar caps area due to two reasons. First, cold accretion disc can penetrate deeper into the neutron star magnetosphere in comparison to the ionised state (see Section 3.3). Second, the accretion from the cold disc on to a slowly rotating neutron star can be accompanied by Rayleigh-Taylor instability at the inner radius (Arons & Lea 1976, 1980). In this case the accretion process is dominated by mass transfer through the diamagnetic filaments falling between magnetic field lines at large latitudes. In this case the area of the polar caps can be very large.

Increase of the size of the polar cap regions is accompanied by the softening of the emerging energy spectrum as seen in the middle panel of Fig. 1. In relatively faint XRPs (with luminosity below the critical value; Mushtukov et al. 2015) the emerging spectrum originates from an optically thin layer at the neutron star surface. The spectrum hardness is determined by the Comptonization y-parameter (Zel'dovich & Shakura 1969), which is given by the product of the average fractional change of photon energy due to single scattering and the average number of scatterings $y = (kT/m_\mathrm{e}c^2)\tau$. The column density of plasma required to slow down the protons in the accretion flow depends only on proton's kinetic energy (Frank et al. 2002). Hence, the average number of photon scatterings is defined by the free-fall velocity and the mechanism of opacity. The temperature is determined by the mass accretion rate. The lower the mass accretion rate we have, the lower the temperature and y-parameter are and, hence, the softer the emerging X-ray spectrum would be. Unfortunately, due to absence of the detailed model of spectrum formation in XRPs, we cannot provide quantitative estimates leaving them for the future papers.

4. Conclusion

In this paper we analysed the *Swift*/XRT observations of GRO J1008−57 obtained between two subsequent Type I outbursts in January and September 2016. The original idea was to detect the transition of the source to the propeller regime accompanied by an abrupt decrease of the source flux and softening of its spectrum. However, during the declining phase of the outburst the source surprisingly stopped its fading and entered a stable accretion state characterized by the accretion rate of the order of $\sim 10^{14} - 10^{15}$ g s^{-1} and hard spectrum. We associate this state with the accretion from cold (non-ionised) disc with temperature below ~ 6500 K.

The model of accretion from the cold disc in the systems harbouring neutron stars with strong magnetic field (i.e. XRPs) is proposed. The basic idea of the model is that in slowly rotating neutron stars the centrifugal barrier caused by the rotating magnetosphere is greatly suppressed in comparison to the fast rotating ones leading to much lower threshold luminosity for the transition to the propeller regime. This fact allows such sources to reach so low mass accretion rates that the temperature throughout the accretion disc becomes lower than the hydrogen recombination limit of ~ 6500 K.

Once this mass accretion rate is reached the fast fading of the source intensity should stop and further accretion with low rate in the stable accretion regime from the cold disc with very low viscosity shall continue. Such behaviour was observed in the pulsar GRO J1008−57 between two consequent Type I outbursts in January and September 2016.

Our model has strong predictive power. Particularly, transition to the accretion regime from a cold disc should be observed in all XRPs with a certain combination of pulse period and magnetic field strength. Moreover, the propeller effect will be never observed in such sources even for very low mass accretion rates. Another prediction concerns the spin-up / spin-down of the neutron star. Obviously, the ongoing accretion in the quiescent state will strongly affect the spin evolution of XRPs and has to be

taken into account, e.g., for the estimates of equilibrium periods. This prediction was confirmed with the *Fermi*/GBM data showing a consistent acceleration of GRO J1008−57 between outbursts.

Acknowledgements. We are grateful to the Swift team for the execution of our ToO request. This work was supported by the Russian Science Foundation grant 14-12-01287 (SST, AAM, AAL, VS), the Deutsche Forschungsgemeinschaft (DFG) grant WE 1312/48-1 (VFS), the Academy of Finland grant 268740 and the National Science Foundation grant PHY-1125915 (JP). VD thank the Deutsches Zentrums for Luft- und Raumfahrt (DLR) and DFG for financial support (grant DLR 50 OR 0702). We also acknowledge the support from the COST Action MP1304.

References

Arons, J. & Lea, S. M. 1976, ApJ, 207, 914
Arons, J. & Lea, S. M. 1980, ApJ, 235, 1016
Balbus, S. A. & Hawley, J. F. 1991, ApJ, 376, 214
Bellm, E. C., Fürst, F., Pottschmidt, K., et al. 2014, ApJ, 792, 108
Brazier, K. T. S. 1994, MNRAS, 268, 709
Burrows, D. N., Hill, J. E., Nousek, J. A., et al. 2005, Space Sci. Rev., 120, 165
Campana, S., Gastaldello, F., Stella, L., et al. 2001, ApJ, 561, 924
Campana, S., Stella, L., & Kennea, J. A. 2008, ApJ, 684, L99
Cannizzo, J. K. 1996, ApJ, 466, L31
Cash, W. 1979, ApJ, 228, 939
Chen, W., Shrader, C. R., & Livio, M. 1997, ApJ, 491, 312
Cheng, F. H., Horne, K., Panagia, N., et al. 1992, ApJ, 397, 664
Cherepashchuk, A. M. 2000, Space Sci. Rev., 93, 473
Coe, M. J., Bird, A. J., Hill, A. B., et al. 2007, MNRAS, 378, 1427
Cui, W. 1997, ApJ, 482, L163
D'Angelo, C. R. & Spruit, H. C. 2010, MNRAS, 406, 1208
de Jager, O. C., Raubenheimer, B. C., & Swanepoel, J. W. H. 1989, A&A, 221, 180
Evans, P. A., Beardmore, A. P., Page, K. L., et al. 2009, MNRAS, 397, 1177
Frank, J., King, A., & Raine, D. J. 2002, Accretion Power in Astrophysics: Third Edition (Cambridge, UK: Cambridge University Press), 398
Gehrels, N., Chincarini, G., Giommi, P., et al. 2004, ApJ, 611, 1005
Ghosh, P. & Lamb, F. K. 1978, ApJ, 223, L83
Illarionov, A. F. & Sunyaev, R. A. 1975, A&A, 39, 185
Kalberla, P. M. W., Burton, W. B., Hartmann, D., et al. 2005, A&A, 440, 775
Kretschmar, P., Kuehnel, M., Nakajima, M., et al. 2016, The Astronomer's Telegram, 8547
Kuehnel, M., Mueller, S., Kreykenbohm, I., et al. 2012, The Astronomer's Telegram, 4564
Kühnel, M., Müller, S., Kreykenbohm, I., et al. 2013, A&A, 555, A95
Lasota, J. P. 1997, in Astronomical Society of the Pacific Conference Series, Vol. 121, IAU Colloq. 163: Accretion Phenomena and Related Outflows, ed. D. T. Wickramasinghe, G. V. Bicknell, & L. Ferrario, 351
Lasota, J.-P. 2001, New A Rev., 45, 449
Levine, A. M. & Corbet, R. 2006, The Astronomer's Telegram, 940
Lipunova, G. V. 2015, ApJ, 804, 87
Lutovinov, A. A. & Tsygankov, S. S. 2009, Astronomy Letters, 35, 433
Lutovinov, A. A., Tsygankov, S. S., Krivonos, R. A., Molkov, S. V., & Poutanen, J. 2017, ApJ, 834, 209
Lynden-Bell, D. & Pringle, J. E. 1974, MNRAS, 168, 603
Lyubarskii, Y. E. 1997, MNRAS, 292, 679
Meyer, F. & Meyer-Hofmeister, E. 1982, A&A, 106, 34
Meyer, F. & Meyer-Hofmeister, E. 1984, A&A, 132, 143
Mineshige, S., Yamasaki, T., & Ishizaka, C. 1993, PASJ, 45, 707
Mushtukov, A. A., Suleimanov, V. F., Tsygankov, S. S., & Poutanen, J. 2015, MNRAS, 447, 1847
Nakajima, M., Kawase, T., Negoro, H., et al. 2016, The Astronomer's Telegram, 9512
Reig, P. 2011, Ap&SS, 332, 1
Reig, P. & Roche, P. 1999, MNRAS, 306, 100
Revnivtsev, M., Churazov, E., Postnov, K., & Tsygankov, S. 2009, A&A, 507, 1211
Riquelme, M. S., Torrejón, J. M., & Negueruela, I. 2012, A&A, 539, A114
Shrader, C. R., Sutaria, F. K., Singh, K. P., & Macomb, D. J. 1999, ApJ, 512, 920
Smak, J. 1984, Acta Astron., 34, 161
Stella, L., White, N. E., & Rosner, R. 1986, ApJ, 308, 669
Stollberg, M. T., Finger, M. H., Wilson, R. B., et al. 1993, IAU Circ., 5836
Tanaka, T. 2011, MNRAS, 410, 1007
Tsygankov, S. S., Lutovinov, A. A., Doroshenko, V., et al. 2016a, A&A, 593, A16
Tsygankov, S. S., Mushtukov, A. A., Suleimanov, V. F., & Poutanen, J. 2016b, MNRAS, 457, 1101
Walter, R., Lutovinov, A. A., Bozzo, E., & Tsygankov, S. S. 2015, A&A Rev., 23, 2
Warner, B. 2003, Cataclysmic Variable Stars (Cambridge: Cambridge University Press), 592
Yamamoto, T., Mihara, T., Sugizaki, M., et al. 2013, The Astronomer's Telegram, 4759, 1
Zel'dovich, Y. B. & Shakura, N. I. 1969, Soviet Ast., 13, 175

Table 1. *Swift*/XRT observations of GRO J1008−57.

Obs Id	Date	Exposure	$N_{\rm H} = 2.0 \times 10^{22}$ cm^{-2}		Free $N_{\rm H}$	
	MJD	ks	XRT flux[a]	Γ[b]	$N_{\rm H}$	Γ[b]
			10^{-11} erg s^{-1} cm^{-2}		10^{22} cm^{-2}	
00031030028	57408.1683	1.0	142±5	1.2±0.1	1.1±0.2	0.7±0.1
00031030029	57414.4910	1.3	35.5±1.3	1.4±0.1	1.8±0.3	1.2±0.2
00031030030	57421.6127	1.2	20.3±1.5	1.4±0.2	1.3±0.4	1.0±0.3
00031030031	57424.0809	2.5	7.8±0.4	1.3±0.1	1.8±0.2	1.2±0.1
00031030032	57426.0158	1.2	$4.8^{+0.3}_{-0.2}$	1.7±0.1	2.0±0.4	1.7±0.3
00031030033	57428.0596	2.3	$4.6^{+0.2}_{-0.1}$	1.6±0.1	1.7±0.2	1.4±0.2
00031030034	57430.5115	2.7	$5.1^{+0.2}_{-0.1}$	1.5±0.1	2.3±0.3	1.7±0.2
00031030035	57432.5746	2.9	$5.1^{+0.2}_{-0.1}$	1.4±0.1	1.7±0.2	1.2±0.1
00031030036	57434.5145	2.5	4.1±0.2	1.6±0.1	1.7±0.3	1.4±0.2
00031030037	57436.4258	1.3	3.2±0.2	1.7±0.1	1.2±0.3	1.2±0.3
00031030038	57440.8239	2.3	2.8±0.1	1.6±0.1	1.4±0.3	1.2±0.2
00031030040	57448.6581	0.2	$2.8^{+0.8}_{-0.5}$	2.1±0.4	0.4±0.7	1.0±0.7
00031030041	57452.4376	1.3	2.5±0.2	1.7±0.2	2.2±0.5	1.8±0.3
00031030042	57456.4917	1.2	2.3±0.2	1.7±0.2	2.1±0.6	1.7±0.4
00031030043	57464.1391	0.2	$2.0^{+0.5}_{-0.4}$	1.3±0.5	0.4±1.0	0.3±0.9
00031030044	57466.6732	2.4	$3.1^{+0.2}_{-0.1}$	1.6±0.1	2.4±0.3	1.8±0.2
00031030045	57468.2726	1.3	$1.9^{+0.1}_{-0.2}$	1.6±0.2	1.6±0.5	1.3±0.3
00031030046	57472.5946	2.4	1.5±0.1	1.7±0.2	2.1±0.5	1.8±0.3
00031030047	57476.8448	2.6	2.0±0.1	1.8±0.1	1.4±0.3	1.4±0.3
00031030048	57480.1727	1.8	$1.7^{+0.2}_{-0.1}$	1.7±0.2	2.5±0.6	2.0±0.4
00031030049	57488.6718	1.3	1.5±0.1	1.8±0.2	2.4±0.6	2.0±0.4
00031030050	57492.4004	0.6	$2.4^{+0.2}_{-0.3}$	1.7±0.2	1.9±0.7	1.7±0.5
00031030051	57493.4566	1.3	1.5±0.2	2.1±0.2	1.4±0.5	1.7±0.4
00031030052	57497.0396	3.1	1.8±0.1	1.6±0.1	1.9±0.3	1.6±0.2
00031030053	57500.2303	2.9	1.8±0.1	1.6±0.1	1.9±0.4	1.5±0.2
00031030054	57504.3630	2.2	1.9±0.1	1.9±0.1	2.4±0.4	2.0±0.3
00031030055	57508.1415	2.9	1.2±0.1	1.6±0.2	1.9±0.5	1.5±0.3
00031030056	57512.2662	1.9	$1.5^{+0.2}_{-0.1}$	2.1±0.2	1.9±0.5	2.0±0.4
00031030058	57524.0342	2.8	1.2±0.1	2.0±0.2	2.0±0.4	2.0±0.3
00031030059	57528.0203	2.9	1.2±0.1	1.7±0.2	2.7±0.5	2.1±0.3
00031030060	57532.4048	2.9	0.9±0.1	2.0±0.2	1.5±0.5	1.6±0.4
00031030061	57540.3100	1.1	$1.4^{+0.1}_{-0.2}$	1.5±0.3	1.3±0.7	1.0±0.5
00031030062	57546.4969	1.5	1.5±0.1	2.0±0.2	2.1±0.5	2.0±0.4
00031030063	57548.0885	1.6	$1.6^{+0.2}_{-0.1}$	1.9±0.2	2.7±0.7	2.3±0.5
00031030064	57552.0065	2.9	1.1±0.1	1.9±0.2	1.8±0.5	1.8±0.4
00031030066	57560.0381	2.6	1.1±0.1	1.5±0.2	1.9±0.5	1.5±0.3
00031030067	57564.2988	3.0	1.1±0.1	1.5±0.2	1.4±0.4	1.2±0.3
00031030068	57572.2871	1.7	1.0±0.1	1.7±0.2	2.6±1.0	2.0±0.6
00031030069	57576.4712	1.6	0.7±0.1	1.3±0.4	1.4±1.0	1.0±0.7
00031030070	57580.3262	1.0	1.0±0.1	1.8±0.3	4.1±1.3	2.9±0.7
00031030071	57584.3187	1.3	0.9±0.1	1.7±0.3	1.2±0.6	1.1±0.5
00031030072	57588.4948	1.6	1.1±0.1	2.0±0.2	1.9±0.6	1.9±0.4
00031030073	57592.0136	0.1	$1.8^{+1.8}_{-0.7}$	2.2±1.0	2.6±3.2	2.6±2.4
00031030074	57594.2706	1.4	1.1±0.1	1.7±0.3	2.4±0.9	1.9±0.6
00031030075	57596.7272	2.7	$0.66^{+0.08}_{-0.07}$	1.4±0.3	1.5±0.7	1.0±0.5
00031030076	57600.7122	2.6	1.1±0.1	1.7±0.2	2.3±0.6	1.9±0.4
00031030077	57604.6330	3.7	$0.83^{+0.08}_{-0.07}$	1.8±0.2	2.1±0.6	1.9±0.4
00031030078	57608.0913	3.3	$0.81^{+0.08}_{-0.07}$	1.7±0.2	2.6±0.7	2.0±0.4
00031030079	57612.0746	3.4	$0.93^{+0.07}_{-0.08}$	1.2±0.2	1.2±0.4	0.8±0.3
00031030080	57616.2037	3.1	1.1±0.1	1.9±0.2	3.0±0.6	2.4±0.4
00031030081	57626.1855	1.4	$0.7^{+0.2}_{-0.1}$	2.2±0.4	0.7±0.7	1.1±0.7
00031030082	57629.0364	1.7	1.1±0.1	1.6±0.2	1.1±0.5	1.0±0.4
00031030083	57630.1009	1.1	0.9±0.1	1.8±0.3	2.1±0.9	1.9±0.7
00031030084	57631.6256	2.1	1.4±0.1	1.7±0.2	1.3±0.4	1.3±0.3
00031030085	57632.0994	2.8	$0.98^{+0.07}_{-0.09}$	1.5±0.2	1.5±0.5	1.1±0.3
00031030086	57636.4050	0.8	$3.0^{+0.2}_{-0.3}$	1.4±0.2	1.8±0.5	1.3±0.4
00031030087	57640.3242	3.2	$8.7^{+0.4}_{-0.2}$	1.3±0.1	2.6±0.3	1.6±0.2

00031030088	57644.0456	3.4	$14.1^{+0.5}_{-0.4}$	1.2±0.1	2.0±0.2	1.2±0.1
00031030089	57648.6950	3.6	78±2	1.0±0.1	2.0±0.2	0.9±0.1
00031030090	57652.7537	3.3	159±3	1.2±0.1	1.5±0.1	1.0±0.1
00031030091	57656.0031	3.3	308^{+4}_{-5}	1.1±0.1	1.3±0.1	0.7±0.1
00031030092	57660.1913	3.5	360^{+6}_{-5}	1.2±0.1	1.2±0.1	0.7±0.1
00031030093	57664.1124	3.1	219±4	1.0±0.1	1.3±0.1	0.7±0.1
00031030094	57668.5570	3.4	54.9±1.5	1.1±0.1	1.8±0.2	0.9±0.1
00031030095	57672.0878	2.7	$19.1^{+0.6}_{-0.7}$	1.1±0.1	2.0±0.2	1.1±0.1
00031030096	57676.0145	1.2	$9.1^{+0.4}_{-0.6}$	1.2±0.1	1.9±0.4	1.1±0.2
00031030097	57678.0084	1.6	7.1±0.1	1.5±0.1	2.4±0.4	1.7±0.2
			Averaged points			
00031030040-56	–	29.7	1.74±0.04	1.74±0.06	2.06±0.08	1.75±0.09
00031030058-64	–	15.6	1.15±0.05	1.84±0.07	2.0±0.2	1.8±0.2
00031030066-85	–	42.2	0.95±0.03	1.63±0.05	1.9±0.2	1.5±0.1

[a] Unabsorbed flux in 0.5–10 keV energy range derived from the model with fixed absorption value.
[b] Photon index.